ACS OMEGA

http://pubs.acs.org/journal/acsodf

Article

Characterization of Silver Nanoparticle Systems from Microalgae Acclimated to Different CO_2 Atmospheres

Shirley Mora-Godínez, Flavio F. Contreras-Torres, and Adriana Pacheco*

Cite This: *ACS Omega* 2023, 8, 21969−21982

Read Online

ACCESS | Metrics & More | Article Recommendations

ABSTRACT: Green synthesis of metallic nanoparticles using microalgae exposed to high CO_2 atmospheres has not been studied in detail; this is of relevance in biological CO_2 mitigation systems where considerable biomass is produced. In this study, we further characterized the potential of an environmental isolate *Desmodesmus abundans* acclimated to low and high CO_2 atmospheres [low carbon acclimation (LCA) and high carbon acclimation (HCA) strains, respectively] as a platform for silver nanoparticle (AgNP) synthesis. As previously characterized, cell pellets at pH 11 were selected from the biological components tested of the different microalgae, which included the culture collection strain *Spirulina platensis*. AgNP characterization showed superior performance of strain HCA components as preserving the supernatant resulted in synthesis in all pH conditions. Size distribution analysis evidenced strain HCA cell pellet platform (pH 11) as the most homogeneous AgNP population (14.9 ± 6.4 nm diameter, −32.7 ± 5.3 mV) followed by *S. platensis* (18.3 ± 7.5 nm, −33.9 ± 2.4 mV). In contrast, strain LCA presented a broader population where the size was above 100 nm (127.8 ± 14.8 nm, −26.7 ± 2.4 mV). Fourier-transform infrared and Raman spectroscopies showed that the reducing power of microalgae might be attributed to functional groups in the cell pellet from proteins, carbohydrates, and fatty acids and, in the supernatant, from amino acids, monosaccharides, disaccharides, and polysaccharides. Microalgae AgNPs exhibited similar antimicrobial properties in the agar diffusion test against *Escherichia coli*. However, they were not effective against Gram (+) *Lactobacillus plantarum*. It is suggested that a high CO_2 atmosphere potentiates components in the *D. abundans* strain HCA for nanotechnology applications.

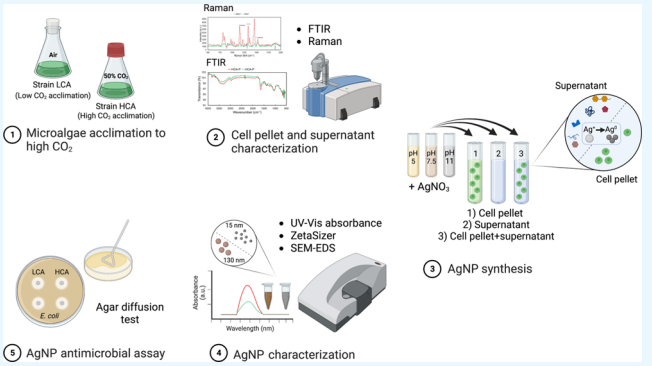

1. INTRODUCTION

Silver nanoparticles (AgNPs) and other metallic nanoparticles are of importance in different fields. The most well-known application is as a non-traditional antimicrobial agent, which shows a broad spectrum of action, including multidrug-resistant bacteria.[1−3] Moreover, AgNPs are studied as carriers for drug delivery, chemical sensing, cosmetics, antioxidants, and others.[4,5] Different preparation routes have been developed, including physical, chemical, or biological approaches. Physical synthesis produces AgNPs on a large scale; however, nanoparticles may aggregate and form large-sized particles. On the other hand, chemical synthesis is the most common method that uses reducing agents such as sodium borohydride and sodium citrate to reduce Ag^+ ions to elemental silver. From a biological approach, plant extracts or microorganisms and their components are used for synthesis, avoiding toxic and hazardous additives or extreme temperature, pressure, and mechanical conditions. The biological method, also known as the green synthesis approach, represents an alternative method that can benefit AgNP production due to its lower cost, environmentally friendly process, and ease of scaling up.[2,4]

The role of microalgae species has received particular attention in the biosynthesis of nanoparticles due to their potential as a versatile renewable resource. Microalgae can be used as reducing agents to yield AgNPs, in which various biological components (e.g., enzymes, polysaccharides, pigments, and peptides) are believed to be responsible for facilitating the reduction process while acting as stabilizers or capping agents.[4,6] The biological effects and factors influencing AgNP activity are discussed elsewhere.[1,4] Noticeably, one of the factors of significant consideration is that nanoparticle properties can be influenced by the microalgae species.[3,7] Green algae and cyanobacteria can provide a sustainable and eco-friendly approach because they are widely used commercially, easy to cultivate, have widespread habitats, and are

Received: March 21, 2023
Accepted: May 23, 2023
Published: June 5, 2023

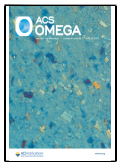

https://doi.org/10.1021/acsomega.3c01914
ACS Omega 2023, 8, 21969−21982

tolerant to extreme conditions.[2,7,8] A second factor in producing nanoparticles with biomass is the use of specific biological components, such as whole cells, extracted molecules, or the supernatant of the culture.[4,7] Finally, a third factor less explored is the potential of microalgae subjected to high CO_2 atmospheres for production of AgNPs. During exposure to high CO_2, tolerant microalgae tend to modify their biochemical composition and concentrate in different cell compartments' reserved molecules such as lipids and carbohydrates.[9,10] For example, carbohydrates have been reported to accumulate in the cell wall,[11] which could benefit the synthesis of AgNPs. The fact that such microalgae can be cultivated for other industrial purposes as for biological mitigation of CO_2 also benefits their use in nanotechnology as an exciting byproduct.

The aim of this study is to further characterize the potential of the environmental isolate *Desmodesmus abundans* as a platform for AgNP synthesis using two strains acclimated and grown in low and high CO_2 atmospheres [strains low carbon acclimation (LCA) and high carbon acclimation (HCA), respectively.] As previously characterized by Mora-Godínez,[12] cell pellets at pH 11 were selected from all biological components and microalgae tested, which included the culture collection strain *Spirulina platensis* (also known as *Anthrospira platensis*) as a positive control. In addition, biological components (cell pellet and supernatant) were comparatively characterized by Fourier-transform infrared (FTIR) and Raman spectroscopies, and the synthesized AgNPs were analyzed using UV−vis and dynamic light scattering. Finally, the antimicrobial potential of the AgNPs was tested using the agar diffusion assay.

2. MATERIALS AND METHODS

2.1. Microalgae Cultures. *D. abundans* RSM (UTEX 2976) isolated from a freshwater sample (Monterrey, Mexico) and acclimated for 12 years to different CO_2 atmospheres[13] was tested after growth in two different conditions: (i) under air CO_2 concentration (0.04% v/v CO_2/air), strain LCA, and (ii) under 50% v/v CO_2/air, strain HCA. Also, *S. platensis* (UTEX LB1926), a culture collection strain commonly used for nanoparticle synthesis,[3,14−16] was used as a positive control. During experimentation, 100 mL of BG-11 medium[17] was inoculated in a 500 mL Erlenmeyer flask to an initial absorbance at 750 nm (Abs750nm) of 0.1 using an active 3/4 log phase culture grown under the same experimental conditions. High CO_2 atmospheres were established by removing through the flasks's rubber stopper the corresponding volume of the headspace with a syringe and adding 99.9% v/v CO_2 (AOC Mexico, Mexico). The low CO_2 condition was achieved using a sterile cotton stopper for proper air exchange as closed cultures do not produce enough biomass for experimentation. Replicate cultures (n = 3) were incubated at 25 ± 2 °C, 60−70 μmol PAR photons m^{-2} s^{-1} of continuous light, and 110 rpm agitation.

Microalgae growth was assessed in 125 mL Erlenmeyer flasks (20 mL working volume) by sacrificing flasks and reading Abs750nm under the linear range of the curve (0.1 to 1.5). Kinetic parameters were determined from the graphical representation of $\ln(X/X_0)$ vs time, where X is the biomass and X_0 is the initial biomass, and the linear range of the curve represented exponential growth.

2.2. Silver Nanoparticle Synthesis. As previously reported by Mora-Godínez,[12] three biological components were tested: (i) cell pellet (pellet), (ii) cell pellet plus supernatant (pellet + supernatant), and (iii) supernatant (supernatant). Culture replicates were grouped as a composite sample, and the cell concentration was normalized based on previous trials starting with Abs750nm of 1.0 and validation of nanoparticle synthesis by solution color, UV−vis absorption spectra, and dynamic light scattering. Abs750nm of 1.0 and 3.0 were established for *S. platensis* and *D. abundans* strains, respectively. Then, three replicates of the normalized cell solution (3 mL) were distributed in clear 15 mL Falcon tubes. Cultures were harvested using a vacuum filtration system and the pellet sample was washed with 100 mL of MilliQ water to remove the supernatant. Afterward, the pellet was resuspended in 10 mL of 10 mM $AgNO_3$ (99.3%; Fermont, Mexico) prepared in MilliQ water. This precursor concentration was previously tested in *Chlorella*,[6] a phylogenetically closed species to *D. abundans*. When preparing the cell pellet plus supernatant sample, the pellet was not washed, and the supernatant was recovered to prepare the $AgNO_3$ solution. This solution also represented the cell-free supernatant treatment. The pH of the solutions was adjusted to pH 5, 7.5, and 11 using 1 N HCl or 1 N NaOH. All experimental solutions were incubated at 25 °C with continuous light for 40 h. Afterward, solutions were filtrated through a 0.2 μm membrane (Corning, NY, USA) for nanoparticle characterization. An abiotic control of $AgNO_3$ solutions in water at different pH was also evaluated.

2.3. Characterization of the Microalgae Biological Material. Samples of the cell pellet and supernatant of each *D. abundans* strain were lyophilized for 48 h or until completely dried and characterized by FTIR and Raman spectroscopies. The vibrational spectra (Spectrum One, PerkinElmer Instruments, USA) were acquired in the transmittance mode at a resolution of 4 cm^{-1} in the range of 500−4000 cm^{-1}. Raman spectra were acquired on a Cora 5500 Raman spectrometer (Anton-Paar, USA) equipped with a diode laser operating at an excitation wavelength of 532 nm and a laser power of 50 mW. Spectra were accumulated over the time of collection at a 3 cm^{-1} spectral resolution. Acquisition time was determined by the software using the implemented auto-exposure option. Also, the options of subtract background and baseline correction were activated with a threshold of 2000 counts, which considers equipment configuration and the nature of the evaluated samples.

2.4. Silver Nanoparticle Characterization. Previous data obtained from the UV−vis absorption spectrum (PerkinElmer Instruments, USA) and ZetaSizer Nano S90 system (Malvern, UK) by Mora-Godínez[12] were used to further analyze and select the most suitable systems.

2.5. Antimicrobial Activity of Silver Nanoparticles. AgNPs synthetized from cell pellets at pH 11, a condition that produced nanoparticles in all species tested, were screened for antimicrobial activity against *Escherichia coli* (ATCC 35218) and *Lactobacillus plantarum* (ATCC 8014) using the plate diffusion test. Bacterial inocula were obtained by culturing frozen stocks in 2 mL of nutrient broth or De Man, Rogosa, and Sharpe medium at 37 °C for 24 h in aerobic and anaerobic conditions for *E. coli* and *L. plantarum*, respectively. Afterward, a subculture was generated using 10% v/v of inocula, and the cells of each culture were harvested in the exponential phase (7−8 h) and adjusted to Abs600nm of 0.1 (8×10^6 CFU mL^{-1}). The cell solution was maintained at 4 °C before testing. Room-temperature agar plates were inoculated with 100 μL of

https://doi.org/10.1021/acsomega.3c01914
ACS Omega 2023, 8, 21969−21982

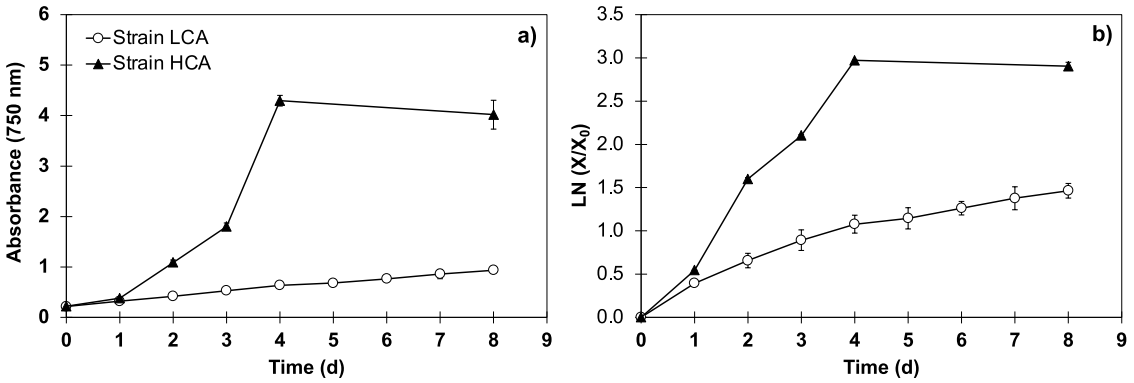

Figure 1. Arithmetic (a) and semi-log (b) growth curves of *D. abundans* strains LCA and HCA in BG-11 medium at 110 rpm, 25 ± 2 °C, and 60−70 μmol PAR photons m^{-2} s^{-1} of continuous light. Values represent average ± SD (n = 3).

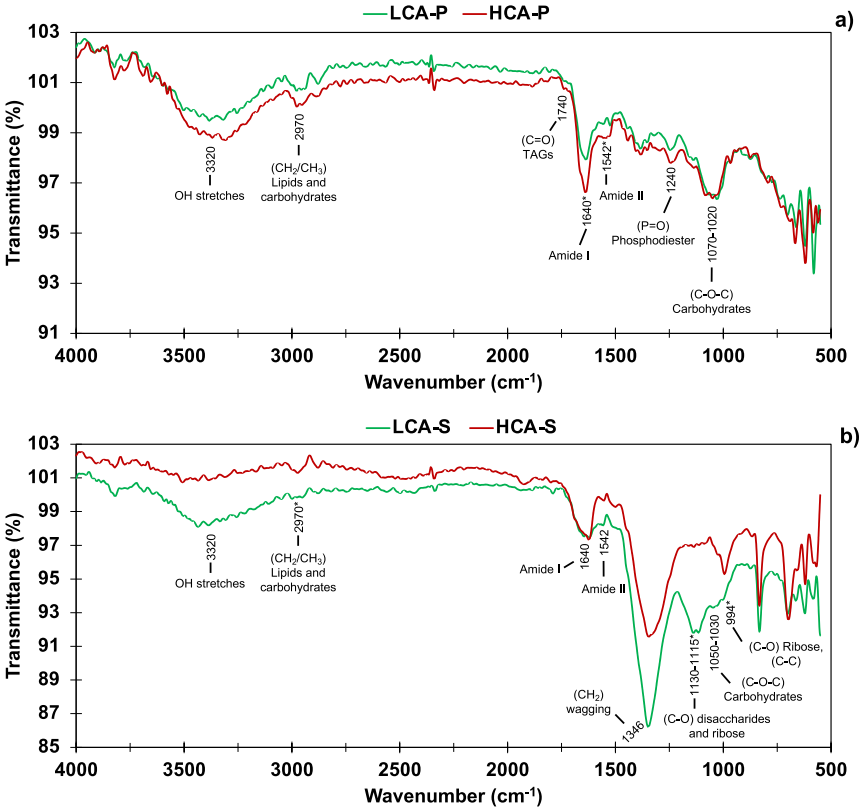

Figure 2. FTIR spectra of *D. abundans* LCA and HCA strains' cell pellets (a) and the supernatant (b). Asterisks indicate differences between strains. P: cell pellet, S: supernatant.

each culture evenly spread with a sterile plastic rod. Then, 100 μL of the AgNPs solution, previously sonicated to resuspend and disaggregate the nanoparticles, was loaded into filter paper discs (Whatman no. 1, 6 mm diameter) or agar wells. Plates were air-dried for approximately 30 min in a biological safety cabinet before incubation. Antimicrobials were tested in triplicate, one disk per plate to account for plate variability. Two positive controls were used for comparison: (i) commercial AgNPs of size <100 nm (99.5%; product no. 576832, Sigma-Aldrich) and (ii) ampicillin sodium salt (≤100%; product no. 69523, Sigma-Aldrich). For the commercial AgNPs, a 1 mg mL^{-1} solution was prepared in MilliQ water and aliquots of 100 μL (100 μg) used as a control. The antibiotic was prepared in water as a 0.5 mg mL^{-1} solution and 20 μL aliquots were used (10 μg). Inhibition zone diameters were measured after 24 h of incubation at 37 °C.

3. RESULTS

3.1. Microalgae as Biological Reducing Agents for the Synthesis of Nanoparticles. The two strains of *D. abundans* were first grown under an atmosphere of air and high CO_2 as shown in Figure 1a,b. Microalgae growth was stimulated under 50% CO_2 where growth rates were approximately 4-fold higher compared to air and corresponded to a higher biomass production. Cultures showed no lag phase, and exponential growth lasted until day 4.

Microalgae components for AgNP synthesis were harvested during exponential growth (day 4) and characterized by FTIR and Raman spectroscopies. Figure 2 shows each strain's

https://doi.org/10.1021/acsomega.3c01914
ACS Omega 2023, 8, 21969−21982

Table 1. FTIR and Raman Band Assignment of *D. abundans* LCA and HCA Strains' Cell Pellets[a]

LCA strain		HCA strain		
FTIR	Raman	FTIR	Raman	band assignment[2,7,18−22]
3320		3320		(OH) stretching of water and polysaccharides
2970		2970		(CH_2) and (CH_3) stretching of lipids and carbohydrates
1740		1740		(C═O) stretching of esters from lipids, i.e., TAGs
1640		1640		(C═O) stretching of amide I from proteins
1542		1542		(N−H) bending and (C−N) stretching of amide II from proteins
	1530		1530	(C═C) carotenoids
	1463		1460	(CH_2) and (CH_3) deformation of lipids (saturated fatty acids)
	1363		1360	guanine and tryptophan
	1330		1330	(CH_3CH_2) wagging mode in purine bases, phosphates, and phospholipids
	1300		1297	(CH_2) deformation of lipids, fatty acids
	ND		1259	guanine, cytosine (NH_2)
1240		1240		(P═O) asymmetric stretching of phosphodiester groups from nucleic acids
	ND		1223	(C−H) ring bend and (PO_2^-) from nucleic acids
	1158		1155	(C−C) and (C−N) stretching of carotenoids and proteins
1070−1030	1038	1070−1020	1038	(C−O−H) deformation, (C−O−C) stretching of polysaccharides from carbohydrates, (P═O) symmetric stretching of nucleic acids, carbohydrates (Raman)
	1003		1003	phenylalanine, (C−C) skeletal
	ND		974	ribose vibration, one of the distinct RNA modes
	ND		945	skeletal modes (polysaccharides, amylose, amylopectin)
	904		904	phosphodiester group, deoxyribose, (C−O−C) skeletal mode, monosaccharide (β-glucose), disaccharide (maltose)
	842		842	glucose, polysaccharide structure
	812		812	phosphodiester group in RNA

[a]ND: Not detected.

Table 2. FTIR and Raman Band Assignment of *D. abundans* LCA and HCA Strains' Supernatants[a]

LCA strain		HCA strain		
FTIR	Raman	FTIR	Raman	band assignment[2,7,18−22]
3320		3320		(OH) stretching of water and polysaccharides
2970		2970		(CH_2) and (CH_2) stretching of lipids and carbohydrates
1640		1640		(C═O) stretching of amide I from proteins
1542		1542		(N−H) bending and (C−N) stretching of amide II from proteins
	1390		ND	(CH) rocking
	1363		1360	guanine and tryptophan
1346		1346		(CH_2) wagging
	1330		1330	(CH_3CH_2) wagging mode in purine bases, nucleic acids, and phosphates
1130−1115		ND		(C−O) of disaccharides and ribose (RNA), (P−O−C) symmetric stretching
1050−1030		1050−1030		(C−O−H) deformation, (C−O−C) stretching of polysaccharides from carbohydrates, (P═O) symmetric stretches of nucleic acids
	1067		1067	(C−C) stretches of fatty acids from TAGs, (C−C) stretching of carbohydrates
ND	ND	994	998	(C−O) ribose
	ND		904	phosphodiester group, deoxyribose, (C−O−C) skeletal mode, monosaccharide (β-glucose), disaccharide (maltose)
	ND		856	amino acids side chain vibrations of proline, hydroxyproline, and tyrosine

[a]ND: Not detected.

vibrational FTIR spectra of the cell pellet (Figure 2a) and supernatant (Figure 2b). In addition, Tables 1 and 2 describe band assignation based on previous reports of macromolecules in microalgae[2,7,18,19] and of biological cell components in general.[20−22] In particular, the cell pellet and supernatant presented characteristic bands of functional groups from lipids and carbohydrates located at ∼3320−2970 cm^{-1}. Typical amide I and II bands were observed at 1640 and 1542 cm^{-1} assigned to C═O stretching and N−H bending, respectively, from the protein's skeleton. In the case of cell pellets, specific bands of esters C═O stretching from lipids such as triacylglycerides (TAGs; ∼1740 cm^{-1}) and phosphodiester groups from nucleic acids (1240 cm^{-1}) were observed. Meanwhile, bands related to carbohydrates were specific to supernatants, namely, 1346 cm^{-1} (CH_2), 1130−1115 cm^{-1} (ribose and disaccharides), and 994 cm^{-1} (ribose). Raman spectroscopy (Figure 3a,b, Tables 1, 2) showed fewer similarities between the cell pellet and supernatant. However, typical bands assigned to vibrations related to carbohydrate structural components such as glucose, maltose, deoxyribose, fatty acids, nucleic acids, and phospholipids were observed around 904, 1300, and 1330 cm^{-1} in both strains' spectra. In particular, Raman spectra for the pellet component showed bands located at approximately 812, 1223, 1259, 1330, and 1360 cm^{-1}, which are assigned to the presence of nucleic acids. A series of low-intensity peaks located at approximately 1155

https://doi.org/10.1021/acsomega.3c01914
ACS Omega 2023, 8, 21969−21982

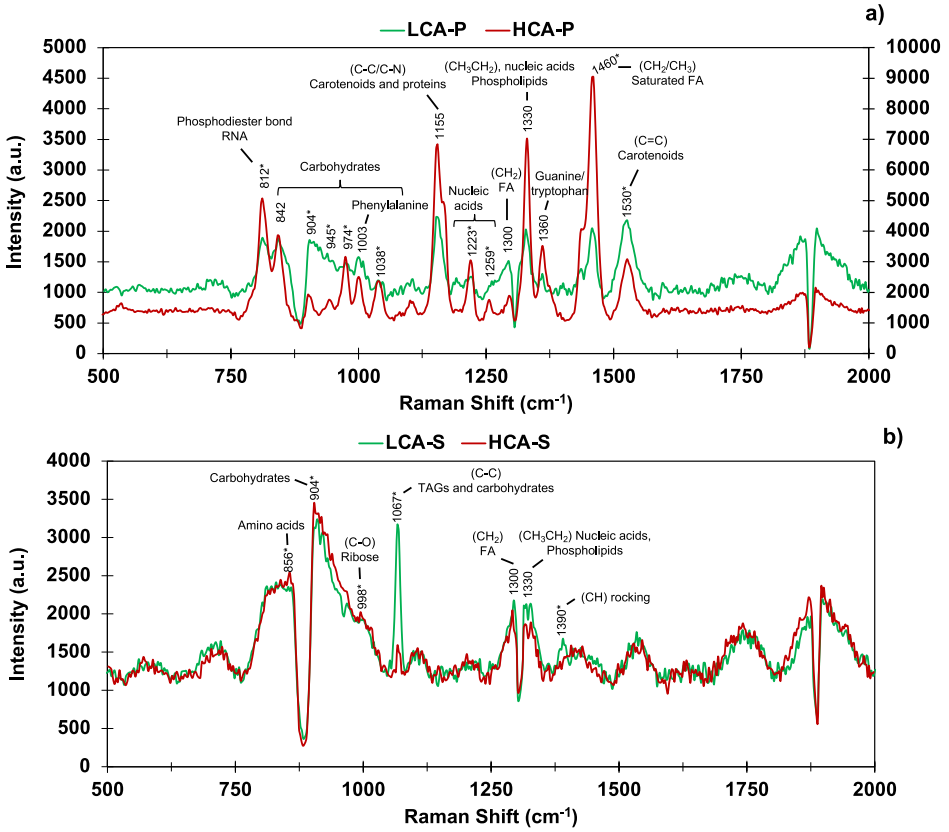

Figure 3. Raman spectra of *D. abundans* LCA and HCA strains' cell pellets (a) and the supernatant (b). Asterisks indicate differences between strains. P: cell pellet, S: supernatant.

and 1530 cm^{-1} (carotenoids), 1300 and 1460 cm^{-1} (lipids), and 842, 904, 945, 974, and 1038 cm^{-1} (carbohydrates) suggest the molecular complexity in the sample. Meanwhile, the supernatant possessed specific bands located at about 856 cm^{-1} (amino acids such as proline and tyrosine), 1067 cm^{-1} (TAGs and carbohydrates), and 998 cm^{-1} (ribose).

Differences between the strains' cell pellets and supernatants were also analyzed by comparing the FTIR and Raman spectra (Figures 2, 3). Cell pellets' FTIR were almost identical except for bands at ∼1542 and 1640 cm^{-1} that showed less transmittance in strain HCA and were assigned to amide I and II from proteins (Figure 2a, Table 1). In the supernatant, a medium intensity band around 1130−1115 cm^{-1} associated with C−O stretching from disaccharide and the ribose structure was only observed in strain LCA (Figure 2b. Table 2). Meanwhile, bands at ∼994 cm^{-1} (ribose) and 2970 cm^{-1} (lipids and carbohydrates) were particular to strain HCA. Raman analysis also showed distinctive bands in the strain HCA cell pellet (Figure 3a). For instance, medium-intensity bands in the range 904−1038 cm^{-1} can be related to monosaccharides (e.g., glucose and ribose), disaccharides (e.g., maltose), and polysaccharides (e.g., amylose and amylopectin from starch), and a low-intensity band in the range 1223−1259 cm^{-1} assigned to nucleic acids (Figure 3a, Table 1). In addition, differences in intensity proportions of two particular bands were also observed to differ between strains; for example, the increase of the band located at ∼812 cm^{-1} (phosphodiester group in RNA) compared to ∼842 cm^{-1} (carbohydrates) and the increase of the band located at ∼1460 cm^{-1} (saturated fatty acids) compared to 1530 cm^{-1} (carotenoids) in the strain HCA cell pellet. In the supernatant, the bands located at 856, 904, and 998 cm^{-1} were only present in strain HCA (Figure 3b, Table 2). These bands can be assigned to the presence of amino acids (e.g., proline and tyrosine) and carbohydrates (e.g., monosaccharides and disaccharides). Conversely, in strain LCA, the band located at 1067 cm^{-1} was more intense than in HCA. This vibrational band can be related to the C−C stretching mode from the presence of fatty acids (e.g., triglycerides). Finally, a band at 1390 cm^{-1} assigned to the C−H rocking from the presence of carbohydrates was only observed in strain LCA.

3.2. Silver Nanoparticle Characterization. Synthesis of AgNPs in the presence of the microalgae biological components was monitored by UV−vis absorbance spectroscopy. Solutions with cell pellets presented an orange-brown color only at pH 11 (Figure 4a,b). However, the color change was more notorious for strain HCA. In accordance, UV−vis absorption spectra for HCA showed a more intense peak around 410 nm (Figure 4b, Table 3). Solutions using the pellet plus supernatant from strain LCA only triggered a change in color to brown at pH 11 (Figure 4c). All solutions from HCA exhibited a color from light brown at pH 5 and 7.5 to dark brown at pH 11 (Figure 4d). Maximum absorbance at 423 nm was observed at pH 11, while a broader range of light absorption (400 to 550 nm) occurred at pH 5 and 7.5 (Table 3). On the other hand, the presence of the supernatant only produced color (dark brown) with strain HCA at pH 11 (Figure 4f). In addition, culture collection species *S. platensis* generated AgNPs in the presence of the cell pellet at all pH values (Figure 5). However, absorbance peaks shifted accordingly to the solution pH, namely, 430 nm for pH 5, 450 nm for pH 7.5, and 410 nm for pH 11 (Figure 5, Table 3).

https://doi.org/10.1021/acsomega.3c01914
ACS Omega 2023, 8, 21969−21982

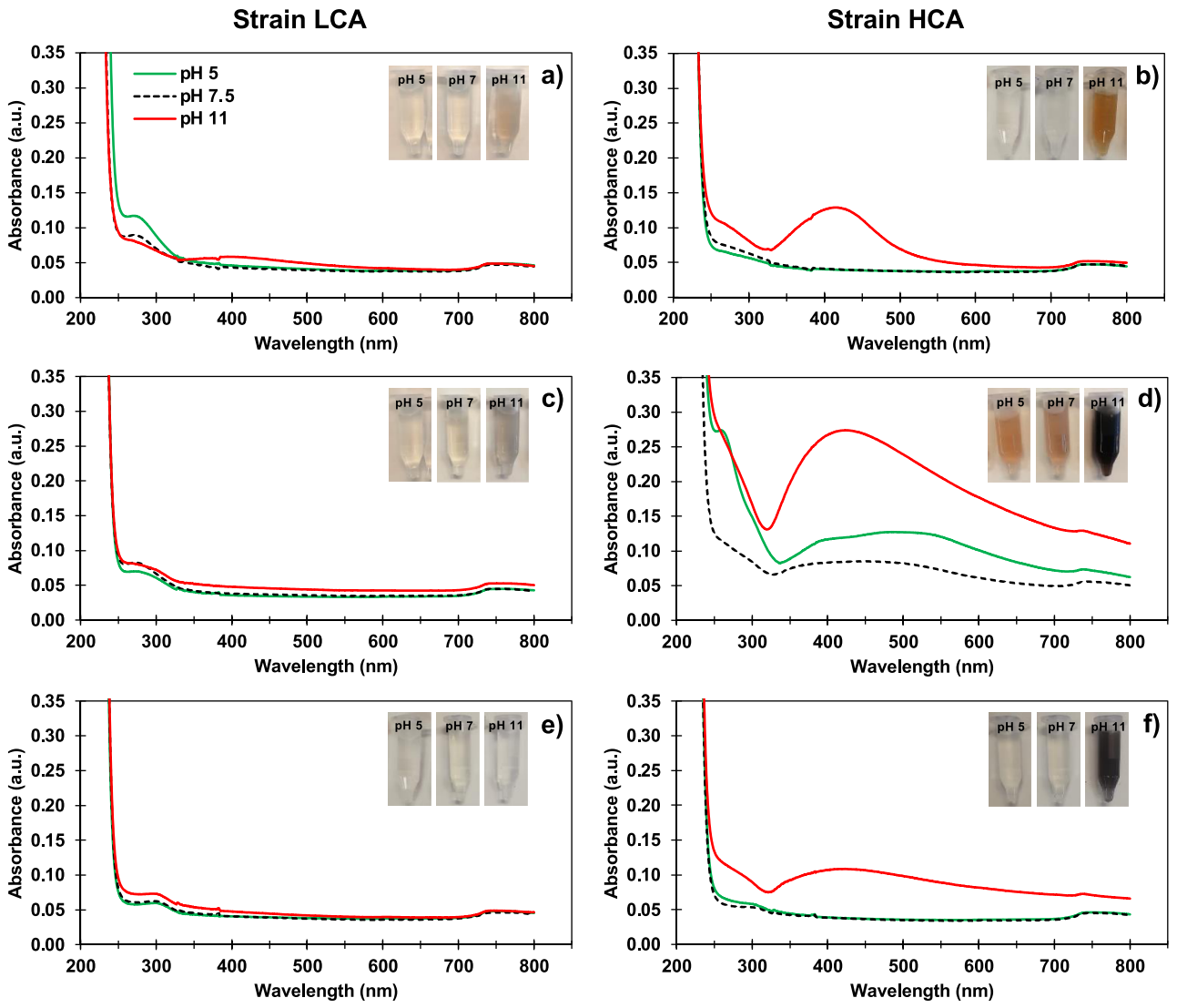

Figure 4. UV−vis absorption spectra of microalgae solutions at different pH using *D. abundans* LCA and HCA strains' cell pellets (a,b), cell pellet plus supernatant (c,d), and supernatant (e,f), respectively. The inset shows the color of solutions after the incubation period. An abiotic control of $AgNO_3$ solutions in water at different pH did not show light absorption (not shown). Reprinted (Adapted or Reprinted in part) with permission from Mora-Godínez, S.; Abril-Martínez, F.; Pacheco, A. Green synthesis of silver nanoparticles using microalgae acclimated to high CO2. *Mater Today: Proc.* **2022**, *48(1)*, 5−9. https://doi.org/10.1016/j.matpr.2020.04.761.[12] Copyright 2022 Elsevier.

Table 3. Characterization of AgNPs from Biological Components of *D. abundans* LCA and HCA Strains' and *S. platensis* Cell Pellets[a]

		λ_{Max} (nm)			size (d, nm)			zeta potential (mV)		
biological component	pH	LCA	HCA	Sp	LCA	HCA	Sp	LCA	HCA	Sp
cell pellet	5	ND	ND	430	ND	ND	130.2 ± 59.6^{A}	ND	ND	−26.5 ± 3.8^{A}
	7.5	ND	ND	450	ND	ND	135.0 ± 54.7^{A}	ND	ND	−28.5 ± 1.0^{A}
	11	395	410	410	127.8 ± 14.8	14.9 ± 6.4	18.3 ± 7.5^{B}	−26.7 ± 2.4	−32.7 ± 5.3	−33.9 ± 2.4^{B}
cell pellet + supernatant	5	ND	486		ND	64.6 ± 15.2^{A}		ND	−14.5 ± 2.2^{A}	
	7.5	ND	468		ND	52.3 ± 28.5^{AB}		ND	−16.6 ± 0.7^{A}	
	11	ND	423		ND	27.7 ± 14.0^{B}		ND	−20.0 ± 1.8^{B}	
supernatant	5	ND	ND		ND	ND		ND	ND	
	7.5	ND	ND		ND	ND		ND	ND	
	11	ND	418		ND	51.8 ± 20.7		ND	−17.4 ± 1.3	

[a]Values represent average ± SD of independent replicates (n = 3). Different letters indicate significant differences among pH conditions for each biological component (Tukey's HSD test, α = 0.05, n = 9). ND: Not detected. Sp: *Spirulina platensis*.

https://doi.org/10.1021/acsomega.3c01914
ACS Omega 2023, 8, 21969−21982

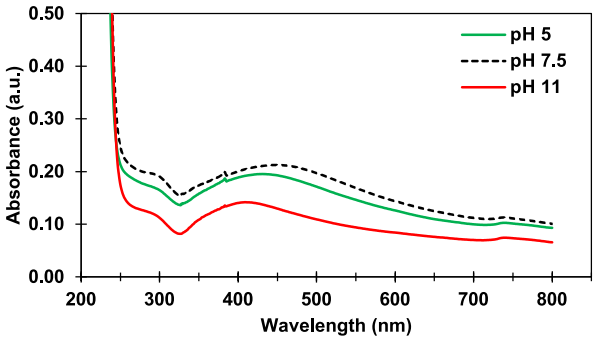

Figure 5. UV−vis absorption spectra of *S. platensis* cell pellet solutions at different pH. Reprinted (Adapted or Reprinted in part) with permission from Mora-Godínez, S.; Abril-Martínez, F.; Pacheco, A. Green synthesis of silver nanoparticles using microalgae acclimated to high CO2. *Mater Today: Proc.* **2022**, *48(1)*, 5−9. https://doi.org/10.1016/j.matpr.2020.04.761.[12] Copyright 2022 Elsevier.

Hydrodynamic particle size and charge characterization of AgNPs from successful experimental conditions are shown in Figure 6 and summarized in Table 3. Nanoparticles from LCA and HCA strains' cell pellets, which only produced nanoparticles at pH 11, showed significant differences in size and charge (*t*-test, α = 0.05, n = 6−9) (Figure 6a,b). The HCA strain presented about a 9-fold smaller diameter of AgNPs (14.9 ± 6.4 nm) than that of the strain LCA (127.8 ± 14.8 nm) and the lowest charge (−32.7 ± 5.3 mV) compared to strain LCA (−26.7 ± 2.4 mV). As mentioned above, when using the cell pellet plus the supernatant, only strain HCA generated AgNPs. Smaller sizes were found at alkaline pH, and AgNP size increased as the pH decreased from pH 11 to 5 (27.7 ± 14.0, 52.3 ± 28.5, and 64.6 ± 15.2 nm, respectively). At pH 11, the average size was around 2-fold smaller than at pH 5 (Tukey's HSD test, α = 0.05, n = 6−9). Similarly, the charge was the lowest at pH 11 (−20.0 ± 1.8 mV) (Tukey's HSD test, α = 0.05, n = 6−9). Using only the supernatant, AgNPs were only detected with strain HCA at pH 11. These nanoparticles did not differ in size nor charge from pellet plus supernatant at pH 11 (*t*-test, α = 0.05, n = 3−9). Overall, AgNPs synthesized using biological components from strain HCA at pH 11 suggest that the supernatant yielded a population of nanoparticles with the largest size and highly variable (51.8 ± 20.7 nm) compared to cell pellets (14.9 ± 6.4 nm) or the pellet plus supernatant (27.7 ± 14.0 nm). Notably, as observed for *D. abundans*, the pH affected the size and

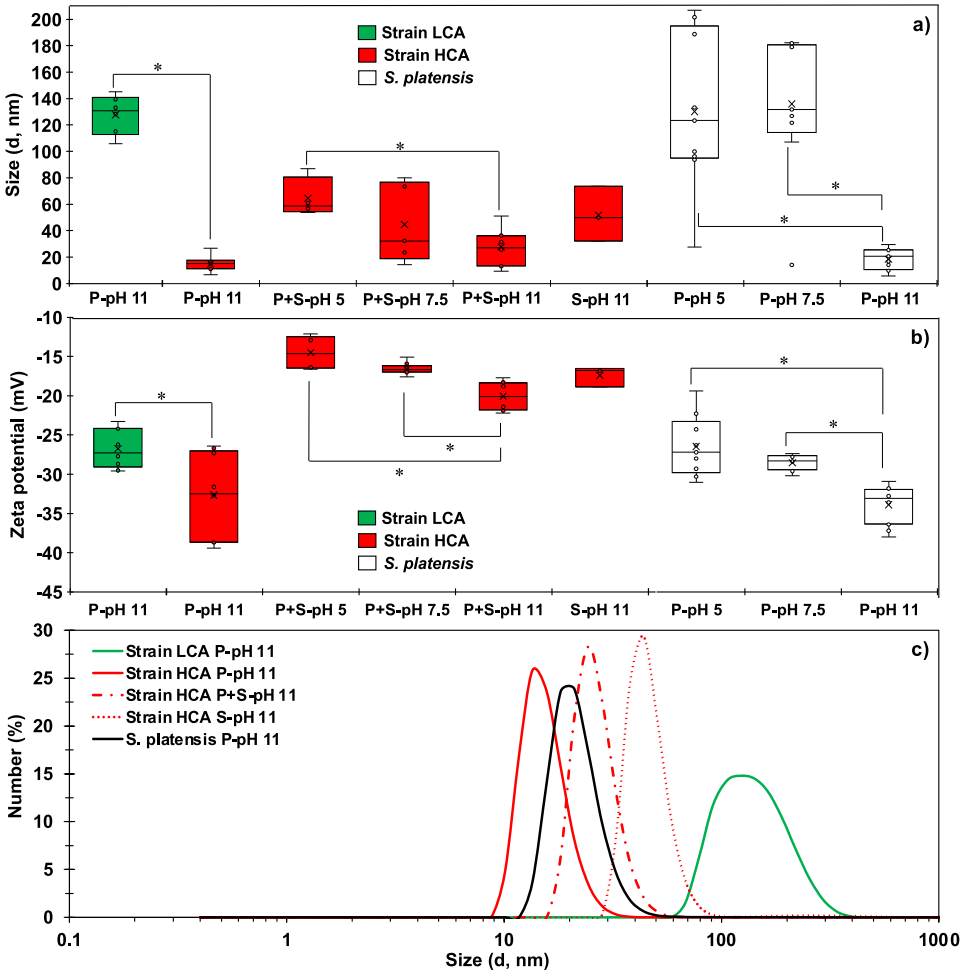

Figure 6. Size (a), charge (b), and size distribution (c) of AgNPs at different pH by dynamic light scattering using *D. abundans* strains LCA and HCA and *S. platensis*. Size distribution of the subset of nanoparticles at pH 11. P: cell pellet, P + S: cell pellet plus supernatant, S: supernatant. Asterisks indicate significant differences (Tukey' HSD test, a = 0.05, n = 9). Reprinted (Adapted or Reprinted in part) with permission from Mora-Godínez, S.; Abril-Martínez, F.; Pacheco, A. Green synthesis of silver nanoparticles using microalgae acclimated to high CO2. *Mater Today: Proc.* **2022**, *48(1)*, 5−9. https://doi.org/10.1016/j.matpr.2020.04.761.[12] Copyright 2022 Elsevier.

https://doi.org/10.1021/acsomega.3c01914
ACS Omega 2023, 8, 21969−21982

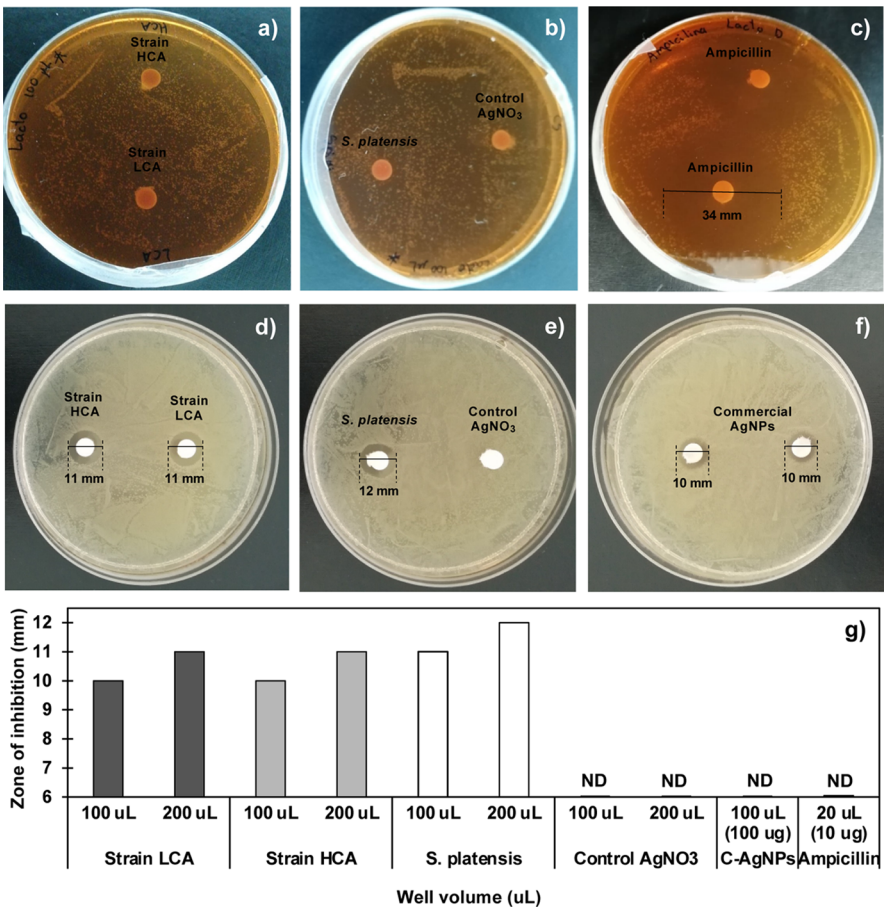

Figure 7. Agar inhibition zones against *L. plantarum* (ATCC 8014) (a–c) and *E. coli* (ATCC 35218) using discs (d–f) and wells (g) of AgNPs obtained with the cell pellet at pH 11 of *D. abundans* LCA and HCA strains, *S. platensis*, control $AgNO_3$ solution, commercial AgNPs (100 μg), and ampicillin (10 μg). Representative agar plates of triplicates. ND: Not detected. C-AgNPs: Commercial solution.

charge of AgNPs from the cell pellet of *S. platensis* (Tukey's HSD test, $\alpha = 0.05$, $n = 6–9$). The smallest AgNPs (18.3 ± 7.5 nm) with the lowest zeta potential value (−33.9 ± 2.4 mV) were observed at pH 11, corresponding to a decrease in size of around 7-fold compared to that of pH 5 and 7.5. Size distribution of the subset of nanoparticles at pH 11, which represents all tested species and the smallest nanoparticles, clearly showed a narrow distribution of size in AgNP populations from strain HCA (15.5 ± 3.8, 26.7 ± 6.3, 45.9 ± 9.8 nm for cell pellet, pellet + supernatant, and supernatant, respectively) and *S. platensis* (21.85 ± 7.2 nm) (Figure 6c) contrary to strain LCA (145.0 ± 53.1 nm) where only the cell pellet generated nanoparticles of a larger size with a broader size distribution.

3.3. Antimicrobial Activity of Silver Nanoparticles. The antimicrobial potential of the AgNPs against *E. coli* and *L. plantarum* was compared using the cell pellet at pH 11, a condition that produced AgNPs in all species tested. Antimicrobial activity against *L. plantarum* was not observed with any of the AgNP samples, while the antibiotic control tested positive (Figure 7a–c). On the contrary, all samples were effective against *E. coli*. AgNPs generated from strains HCA and LCA showed similar antimicrobial activity with inhibition diameters of 11 ± 0 mm (Figure 7d). A slightly higher inhibition zone was observed with *S. platensis* (12 ± 0 mm) (Figure 7e). In addition, the solution control of $AgNO_3$ did not show antimicrobial activity, and the commercial AgNPs (100 μg) as a positive control produced inhibition diameters of 10 ± 0 mm (Figure 7e,f). Similar results were obtained using agar wells even at two times the volume of the test solution (200 μL), which only produced a 1 mm increase in inhibition zones of all samples tested (Figure 7g). Interestingly, in wells, commercial AgNPs did not exhibit inhibition of *E. coli* and the ampicillin amount used (10 μg) was not sufficient to inhibit growth.

4. DISCUSSION

4.1. High CO_2-Tolerant Microalgae as Reducing Agents for the Synthesis of Silver Nanoparticles. Green synthesis of AgNPs represents an environmentally friendly and cost-effective alternative to traditional chemical and physical methods.[16] Notably, green algae and cyanobacteria can offer various reducing agents for AgNP synthesis.[3] Furthermore, green algae species phylogenetically related to the genus *Desmodesmus* have been reported to tolerate high CO_2 atmospheres, mostly around 20% v/v CO_2/air, and increased biomass production and particular reserved molecules that could benefit the synthesis of AgNPs.[9–11,23] This characteristic is of relevance for potential byproducts in CO_2 biomitigation systems.

As expected, a higher growth rate and biomass production was observed under high CO_2 compared to an air atmosphere (Figure 1a,b). Identification of biomolecules present in the biomass (cell pellet) and supernatant of the cultures was

https://doi.org/10.1021/acsomega.3c01914
ACS Omega 2023, 8, 21969–21982

performed using the complementary techniques FTIR and Raman spectroscopy. In FTIR, molecules are excited by absorbing infrared radiation, which provides information about the vibrational modes of the sample. On the other hand, in Raman, the sample is excited by scattering light that characterizes the rotational and vibrational modes of the sample. Therefore, FTIR is useful for identifying functional groups and determining the molecular structure of the sample, while Raman is better suited for identifying specific chemical bonds and detecting impurities in similar samples without the need of destructive and time-consuming analytical techniques.[24] Additionally, when a molecule is Raman active, it is *IR*-inactive and vice versa.[25] From Figures 2a and 3a, it can be stated that the cell pellets possess functional groups assigned to lipids, carbohydrates, proteins, carotenoids, and nucleic acids (Table 1) commonly found in microalgae.[7,18] However, FTIR showed that lipids as TAGs (~1740 cm^{-1}) and phosphodiester groups from nucleic acids (~1240 cm^{-1}) were specific to the cell pellet component. In contrast, supernatants mainly showed bands associated with different types of carbohydrates but also the presence of proteins, lipids, and nucleic acids (Figures 2b, 3b; Table 2). In agreement, it has been reported that microalgae's main extracellular components are exopolysaccharides (EPS), proteins, and small quantities of fatty acids, nucleic acids, and amino acids.[26,27] Production of EPS has been reported as a species-dependent process regulated by growth conditions such as concentration of nitrogen and phosphorus.[2,26,28−31] Excreted proteins function as structural components for EPS stabilization and enzymes involved in EPS degradation, C-capture, and protein degradation, among others.[26,27]

Differences between strains from the FTIR spectra analysis of the cell pellets showed the presence of amide I and II from proteins in strain HCA (Figure 2a). On the other hand, Raman analysis also showed some unique and more intense peaks in strain HCA, assigned to groups from nucleic acids and saturated fatty acids (Figure 3a). In the supernatants, FTIR spectra showed that strain LCA presented at 1130−1115 cm^{-1} a band related to sugars such as disaccharides and ribose (Figure 2b). In addition, Raman spectra exhibited bands only manifested in strain HCA assigned to amino acids (e.g., proline and tyrosine), monosaccharides (e.g., glucose and ribose), and disaccharides (e.g., maltose) (Figure 3b). However, strain LCA showed a very intense band assigned to C−C stretching from fatty acids in TAGs and carbohydrates (~1067 cm^{-1}) and a band at approximately 1390 cm^{-1} (C−H rocking), which was not identified in strain HCA.

Higher metabolic activity is expected in strain HCA because of growth in an enriched CO_2 atmosphere compared to strain LCA grown under air. Under 50% CO_2, excess carbon was used for cell growth, generating more biomass and producing extracellular metabolites. It is important to mention that when the supernatant from HCA was prepared for analysis, a portion was retained in the filter, suggesting the presence of large molecules, which were not considered. In contrast, under an air atmosphere, strain LCA seems to deal with low CO_2 concentrations by excreting storage metabolites like TAGs and carbohydrates such as disaccharides and ribose. However, the presence of these molecules in the supernatant was not sufficient to generate nanoparticles or they inhibit the process as only the supernatant from strain HCA produced AgNPs (Figure 6). Therefore, it seems that the presence of amino acids or the type of carbohydrates in strain HCA, as they showed different FTIR and Raman spectra, made the difference.

4.2. Characterization of Biologically Synthesized Silver Nanoparticles. AgNP formation using different biological components from *D. abundans* strains was evaluated at different pH values (Figure 4). Biotransformation of Ag^+ to Ag^0 can be characterized by the response to the surface plasmon of silver and the appearance of an orange-brown color, which absorbs light at a wavelength of 400−450 nm.[2,6−8] In addition, scanning electron microscopy and energy-dispersive X-ray spectroscopy confirm the presence of elemental silver in nanoparticles by a typical 2.98 keV signal.[2] Accordingly, previous data by Mora-Godínez[12] confirmed the presence of AgNPs using these two sets of data in both microalgae strains cell pellet samples at pH 11 (Figure 4a,b). Nevertheless, the other biological components at pH 11 led to AgNP synthesis only in strain HCA (Figure 4b,d,f). Overall, strain HCA solutions were more intense in color and presented higher absorbances than strain LCA (Table 3).

The superior performance of biological components of strain HCA to generate AgNPs is probably caused by a higher content of functional groups that act as reducing agents of Ag^+ ions (Figures 2, 3, Tables 1, 2). Previous studies have used different components of microalgae for nanoparticle synthesis (Table 4). For example, Kashyap[7] and Castro[32] achieved AgNP formation using an ethanolic extract of the biomass or dried ground biomass , respectively. They characterized the functional groups involved in biosynthesis by FTIR. Reduction of silver was proposed to occur by vibrational bands corresponding to amides (N−H), carbohydrates (CH_2 and CH_3), and lipids (C═O and O−H), which can also act as capping agents. In this study, FTIR and Raman analysis showed the presence of bands for amide I and II as well as bands from carbohydrates and saturated fatty acids in the cell pellets (Figure 2a, 3a). Such assignment can be associated with the cell wall of the microalgae, which is rich in polysaccharides that possess these functional groups.[32] Therefore, the higher capacity of strain HCA grown under 50% CO_2 could be associated with a higher content of hydroxyl, carboxylic, and aldehyde groups in the cell wall. In accordance, previous studies have reported an increase in polysaccharide content in microalgae cell walls under high CO_2 as a sink for excessive photosynthate production.[9,11] Also, antioxidants from microalgae, for example, pigments, could play a key role in AgNP synthesis. Patel[3] reported that phycocyanin extracted from cyanobacteria could generate AgNPs in the presence of light, but the mechanism is still not known. In this study, synthesis was conducted under light, and carotenoids were detected as part of the cell pellet of both strains. Hence, under high CO_2, pigments and other antioxidants are probably in higher concentrations as cells are actively growing.

On the other hand, the pellet plus supernatant from strain LCA only triggered the formation of AgNPs to a low extent at pH 11, contrary to strain HCA, which generated AgNPs in all pH values (Figure 4c,d). For strain HCA, the AgNPs showed maximum absorbance at pH 11, where the solution turned a dark color, which suggests that this component possessed a reducing potential for nanoparticle formation. Neither the pellet nor the supernatant can produce AgNPs at pH 5 and 7.5; however, combining these two components appeared to increase the reducing power, achieving nanoparticle formation (Figure 4d).

https://doi.org/10.1021/acsomega.3c01914
ACS Omega 2023, 8, 21969−21982

Table 4. Characteristics of Microalgae-Mediated AgNP Synthesis and Antimicrobial Activity

	nanoparticle synthesis			antimicrobial activity		
species	biological component	synthesis conditions	size[a](nm)	method[b]	pathogen	reference
green algae						
Chlorella sp	ethanol extract	0.5 mM $AgNO_3$, pH 7.37, 28 °C, 192 h	10−20	agar well diffusion (20 μL)	G+: *Bacillus subtilis, B. sphaericus, B. pasteurii*; G−: *E. coli*	7
Scenedesmus vacuolatus	ethanol extract	0.5 mM $AgNO_3$, pH 7.37, 28 °C, 192 h	136.2	ND	ND	7
Desmodesmus sp	viable cells (intracellular)	5 mM $AgNO_3$, pH 8, 28 °C, 72 h	15−30	ND	ND	33
Chlorella vulgaris	viable cells	10 mM $AgNO_3$, pH 5, 7.5 &; 10, 25 °C, 48h	10	MIC (0−100 μg mL^{-1})	G+: *Staphylococcus aureus* (>50 μg mL^{-1})	6
Botrycoccus sp	viable cells	1 mM $AgNO_3$, pH 7, light, 25 °C, 72 h	15.67 ± 1	agar well diffusion (70 μL)	G+: *Bacillus megaterium, Bacillus subtilis, Staphylococcus aureus, Micrococcus luteus*; G−: *E. coli, Pseudomonas aeruginosa*	3
Spyrogira insignis	ground biomass	5 mM $AgNO_3$, pH 4, 6 &; 10	30	ND	ND	32
Scenedesmus abundans	aqueous extract	1 mM $AgNO_3$, 25 °C, 48 h	150	agar well diffusion (25, 50, 75, 100 μL)	G−: *E. coli, Klebsiella pneumonia, Aeromonas hydrophila*	8
Scenedesmus sp	intracellular	5 mM $AgNO_3$, 28 °C, 22 h	15−20	agar well diffusion (10, 20, 30, 40 μL)	G+: *Streptococcus mutans*; G-: *E.coli*	34
	34					
	boiled extract	5 mM $AgNO_3$, incubated until color change	5−10	agar well diffusion (10, 20, 30, 40 μL)	G+: *Streptococcus mutans*; G-: *E. coli*	34
	34					
Coelastrum sp	biomass	1 mM $AgNO_3$, pH 7, light or dark, 25 °C, 72 h	19.28 ± 1	agar well diffusion (70 μL)	G+: *Bacillus megaterium, Bacillus subtilis*; G−: *Pseudomonas aeruginosa*	3
Botryococcus braunii	EPS	Continuous addition of 3.5 mM $AgNO_3$, pH 8, 90 °C, 1 h	13.8 ± 5.3	MIC (0.5−40 μg mL^{-1})	G+: *Staphylococcus aureus* (30 μg mL^{-1}), *Staphylococcus aureus* MRSA (40 μg mL^{-1}); G−: *E. coli* (>7.5 μg mL^{-1})	2
Chlorella pyrenoidosa	EPS	Continuous addition of 3.5 mM $AgNO_3$, pH 8, 90 °C, 1 h	9.2 ± 4.2	MIC (0.5−40 μg mL^{-1})	G+: *Staphylococcus aureus* (30 μg mL^{-1}), *Staphylococcus aureus* MRSA (30 μg mL^{-1}); G−: *E. coli* (7.5 μg mL^{-1})	2
Chlorella vulgaris	supernatant	5 mM $AgNO_3$, 50 °C, 24 h	9	MIC (2.35−300 μg mL^{-1})	G+: *Staphylococcus aureus* (37.5 μg mL^{-1}); G−: *E. coli* (9.4 μg mL^{-1})	35
Coelastrella aeroterrestrica	aqueous extract	10 mM $AgNO_3$, light, RT, 24 h	28.5	MIC (<0.98−1.95 μg mL^{-1}), MBC (<0.98−3.9 μg mL^{-1}), agar well diffusion (50 μg)	G+: *Staphylococcus aureus, Streptococcus pyogenes, B. subtilis*; G−: *E. coli, P. aeruginosa*	36
Unicellular *Ulvophyte sp*	aqueous extract	1, 2, 5 &; 10 mM $AgNO_3$, 25 °C, 24 h	178.1	agar well diffusion (1 mg mL^{-1})	G+: *B. subtilis, B. cereus*; G−: *E. coli, K. pneumoniae*	37
Desmodesmus abundans strain LCA	cell pellet	10 mM $AgNO_3$, pH 5, 7.5 &; 11, light, 25 °C,40 h	128 ± 15 (pH 11)	agar disc diffusion (100 μL)	G+: *Lactobacillus plantarum*; G−: *E. coli*	this study
Desmodesmus abundans strain HCA	cell pellet	10 mM $AgNO_3$, pH 5, 7.5 &; 11, light, 25 °C, 40 h	15 ± 6 (pH 11)	agar disc diffusion (100 μL)	G+: *Lactobacillus plantarum*; G−: *E. coli*	this study
	Cell pellet + supernatant		65 ± 15 (pH 5), 52 ± 29 (pH 7.5), 28 ± 14 (pH 11)	ND	ND	this study
	supernatant		52 ± 21 (pH 11)	ND	ND	this study
cyanobacteria						
Spirulina platensis	viable cells	1, 2 &; 3 mM $AgNO_3$, pH 7, 25 °C, 24 h	11.5	agar well diffusion (40, 60, 80, 100 μL)	G+: *Staphylococcus aureus, Staphylococcus epidermidis*; G−: *Klebsiella pneumonia, E. coli, Pseudomonas aeruginosa*	14
Nostoc sp	viable cells	1, 2 &; 3 mM $AgNO_3$, pH 7, 25 °C, 24 h	20.3	agar well diffusion (40, 60, 80, 100 μL)	G+: *Staphylococcus aureus, Staphylococcus epidermidis*; G−: *Klebsiella pneumonia, E. coli, Pseudomonas aeruginosa*	14
Lyngbya putealis	ethanol extract	1 mM $AgNO_3$, pH 7.4, 28 °C	241.8	ND	ND	7

https://doi.org/10.1021/acsomega.3c01914
ACS Omega 2023, 8, 21969−21982

Table 4. continued

species	nanoparticle synthesis: biological component	nanoparticle synthesis: synthesis conditions	nanoparticle synthesis: size[a] (nm)	antimicrobial activity: method[b]	antimicrobial activity: pathogen	reference
cyanobacteria						
Spirulina platensis	aqueous extract	1 mM $AgNO_3$, pH 5, 6, 7 &; 8, 0−12 h	5−50	MIC (1−4 mM)	G+: *Staphylococcus sp*; G−: *Klebsiella sp*	16
Spirulina platensis	cell pellet	10 mM $AgNO_3$, pH 5, 7.5 &; 11, light, 25 °C, 40 h	18 ± 8 (pH 11)	agar disc diffusion (100 μL)	G+: *Lactobacillus plantarum*; G−: *E. coli*	this study
			130 ± 60 (pH 5), 136 ± 55 (pH 7.5)	ND	ND	this study

[a]Diameter using microscopic techniques or zeta sizer. [b]In parenthesis, volume or concentration used in the test. MIC: Minimum inhibitory concentration. MBC: Minimum bactericidal concentration. G +: Gram +, G−: Gram −. ND: Not determined.

Synthesis of AgNPs in the supernatants was attributed to functional groups from amino acids (e.g., proline and tyrosine), carbohydrates (e.g., glucose, maltose, and polysaccharides), and ribose as the observed vibrational bands at 856, 904, and 998 cm^{-1}, respectively (Figure 3b, Table 2). Moreover, EPS from microalgae are known to potentiate the formation of AgNPs.[2,3,35] EPS are even proposed as responsible for AgNP synthesis in green microalgae.[3] The higher capacity of strain HCA to produce AgNPs is probably because of the excess of carbon assimilated by the microalgae, potentially representing higher concentrations of reducing agents in this biological component.

Culture collection strain *S. platensis* was only tested using the cell pellet as a microalga biomass commonly reported for nanoparticle synthesis.[3,14−16] AgNP formation was observed in all pH solutions, but at pH 5 and 7.5, the UV−vis spectrum shifted toward 450 nm compared to pH 11's narrower peak and maximum absorbance at 410 nm (Figure 4, Table 3). A previous study with *Spirulina* showed similar results, where at neutral and alkaline pH, a narrower band in the UV−vis spectrum was observed.[16] This effect is also observed in strain HCA using the pellet plus supernatant at pH 5 and 7, which showed a wider range of absorption (400−550 nm; Figure 4d). Navarro-Gallón[2] explained this result concerning how morphology and size of AgNPs influence light absorption. Commonly, a symmetric peak indicates the presence of isotropic particles with a more homogenous size distribution. In agreement, size distribution of the subset of AgNPs of strain HCA and *S. platensis* at pH 11 also showed narrow peaks (Figure 6c). At pH 5 and 7.5, nanoparticle size represented by boxplots showed a wider size range (Figure 6a). Therefore, the pH of the solution plays an essential role in the reducing and stabilizing potential of the biological component tested in this study. Other studies have also suggested the dependence on alkaline pH values for AgNP synthesis.[4,32] The authors explained that there is competition between protons and Ag^+ cations at low pH, while at higher pH, OH^- ions tend to agglomerate nanoparticles, improving their stability.

D. abundans strains generated AgNPs with cell pellets at pH 11 that significantly differ in size, about 9-fold smaller with strain HCA than with strain LCA (14.9 ± 6.4 and 127.8 ± 14.8 nm, respectively). Their size distribution clearly separates two populations, one of a small homogenous size and the other of a wide range of large particles (Figure 6, Table 3). This result suggests differences between the strain's cell pellet composition, as previously mentioned, mainly the presence of some unique and more intense bands of functional groups of proteins (amide I and II), nucleic acids, and saturated fatty acids in strain HCA compared to strain LCA. On the other hand, nanoparticles with strain HCA supernatant were larger, presented a broader size distribution, and had the highest ZP (less negative) than when using only the cell pellet or pellet plus supernatant at pH 11. Therefore, it seems as if the reducing and capping agents were less effective when the supernatant was incorporated at this pH. However, our results showed that both biological components from high CO_2 growth conditions have the potential to generate AgNPs. Further optimization could improve results using the supernatant, which seems effective at lower pH values combined with the cell pellet.

High charge values can be correlated to the presence of sugars and proteins that cap the nanoparticle surface, providing stability.[35] FTIR and Raman analysis suggest the presence of

https://doi.org/10.1021/acsomega.3c01914
ACS Omega 2023, 8, 21969−21982

these macromolecules in the supernatant of strain HCA. However, carbohydrates were also detected in the supernatant of strain LCA, where no indication of nanoparticle production was observed according to spectroscopy measurements. This result might be considered an effect of the low CO_2 growth condition since both biomass samples were normalized before synthesis. We note that it can also be explained by a particular sugar or protein associated with each strain. In addition, it appears that the lowest ZP was observed in the smallest AgNPs as the pH of the solution increased to alkalinity. It has been reported that ZP varies widely among species and synthesis conditions. For example, Navarro-Gallón[2] reported values of −12.2 mV for *Chlorella* and −51.8 mV for *Botryococcus* using purified EPS.

In agreement with other reports (see Table 4), AgNP characteristics depended on microalgae species, the biological component used, and the pH of the solution.[6,7] These effects result in a wide range of nanoparticle sizes reported for phylogenetically close species of green algae (5−178 nm)[2,3,6−8,32−37] and cyanobacteria (5−242 nm).[7,14−16]

4.3. Antimicrobial Activity of Silver Nanoparticles. AgNP antimicrobial properties are commonly tested as a means to potential application. In the present study, AgNPs synthesized from the cell pellet at pH 11, which yielded nanoparticles in all microalgae species tested, showed similar antimicrobial activity against *E. coli* using the agar diffusion method (Figure 7). However, AgNPs were not effective to control the Gram (+) reference strain, *L. plantarum*. This is a fermentative bacterium that grows under anaerobic conditions, which might limit AgNPs' mechanism of action if it depends solely on targets associated with oxygen respiration.[1] Also, it has been reported that nanoparticles synthesized from microalgae can show different antimicrobial spectrums. Patel[3] tested eight different microalgae-synthetized AgNPs and only half of them were effective to all bacteria tested, including Gram (+) and Gram (−).

Against *E. coli*, *S. platensis* showed a slightly higher inhibition zone of 12 mm compared to *D. abundans* strains (11 mm) and commercial AgNPs at 100 μg (10 mm). Different protocols have been used to test AgNPs' antimicrobial potential based mainly on estimated or indirect nanoparticle concentrations (Table 4). Because the agar diffusion assay is qualitative and depends on many factors, such as the solubility of the antimicrobial compound on the agar medium, comparisons among studies are difficult. In the case of *E. coli*, our study evidenced that the diffusion of the AgNP solutions was greatly affected by the delivery method as in wells, the same volume of nanoparticles produced lower inhibition zones and even the commercial AgNPs showed no activity; probably they form aggregates in the plate surface (Figure 7b).

Studies where nanoparticle concentration was determined report promising minimum inhibitory concentration (MIC) values for representative Gram (+) and Gram (−) bacteria; the latter group is considered difficult to control because of the multiple layers that compose the cell wall. Still, AgNPs appear to be especially effective against this group of bacteria. As shown in Table 4, the MIC for *Staphylococcus aureus* is in a range of >50 to 30 μg mL^{-1}, while for *E. coli*, from 9.4 to 7.5 μg mL.[2,6,35] The mechanism of antimicrobial action of AgNPs can be related to three main mechanisms: (i) cell membrane destabilization and damage, (ii) internal interaction with sulfur- and phosphorus-containing groups of macromolecules such as proteins and DNA, or even with thiol-containing enzymes in the respiratory membrane chain inducing the formation of reactive oxygen species and free radicals, and (iii) in parallel with the other two mechanisms, releasing silver ions, which can interfere with essential processes involved in gene expression, protein synthesis, and respiratory membrane chain destabilization that result in cell death.[1,2,6,8,35]

The size and charge of the particles constitute a significant property of AgNPs related to their antimicrobial efficacy. Small nanoparticles present a larger surface area, leading to more significant interactions with bacteria and their molecular components.[6,7] However, particle charge determines the stability of the nanoparticles, being below −30 mV and above +30 mV conditions that prevent their agglomeration.[1] In this study, AgNPs obtained with *D. abundans* strains HCA (15 ± 6 nm, −33 ± 5 mV) and LCA (128 ± 15 nm, −27 ± 2 mV) showed similar inhibitory activity despite significant differences in size. Also, *S. platensis* AgNPs exhibited slightly higher inhibition than strain HCA regardless of presenting similar size particles and charge (18 ± 8 nm, −34 ± 2 mV). However, a significant result is that microalgae-based syntheses showed superior antimicrobial activity than commercial AgNPs (100 ppm). Commercial AgNPs seemed to aggregate in wells, impairing their antimicrobial activity. Therefore, it is suggested that not only AgNP properties of size and charge influence antimicrobial activity but also the presence of capping molecules and the environment in which nanoparticles form the colloids. Table 4 shows a wide range of sizes with reported antimicrobial activity where most particles are <30 nm, but there are also reports of up to 150 nm. Accordingly, the antimicrobial activity of AgNPs can be improved by considering other physical parameters such as shape and capping molecules that seem to be particular factors of the biological component used for nanoparticle synthesis.

5. CONCLUSIONS

Differences between *D. abundans* strains grown in high and low CO_2 atmospheres (strains HCA and LCA, respectively) were observed concerning their composition and synthesis of AgNPs. All biological components of strain HCA grown under 50% v/v CO_2/air generated AgNPs. In contrast, only the cell pellet of strain LCA produced particles of considerable size (9-fold larger than strain HCA). Higher reducing power in strain HCA biomass might be attributed to functional groups from proteins, carbohydrates, and fatty acids. The presence of reducing agents such as amino acids, monosaccharides, disaccharides, and polysaccharides is suggested in the supernatant. In general, the cell pellet platform under highly alkaline pH produced AgNPs in all microalgae tested. Size distribution analysis evidenced the strain HCA cell pellet (pH 11) as the most homogeneous AgNP population (14.9 ± 6.4 nm diameter, −32.7 ± 5.3 mV) followed by *S. platensis* (18.3 ± 7.5 nm, −33.9 ± 2.4 mV). In contrast, strain LCA presented a broader population where the size was above 100 nm (127.8 ± 14.8 nm, −26.7 ± 2.4 mV). These samples from three microalgae strains showed similar antimicrobial properties against *E. coli* in the agar diffusion test. However, they were not effective against Gram (+) *L. plantarum*. These results suggest that microalgae under high CO_2 atmospheres represent a valuable platform for green synthesis of metallic nanoparticles with specific antimicrobial properties. Further studies should clarify the antimicrobial spectrum of the synthesized AgNPs.

https://doi.org/10.1021/acsomega.3c01914
ACS Omega 2023, 8, 21969−21982

AUTHOR INFORMATION

Corresponding Author

Adriana Pacheco − *Tecnologico de Monterrey, Escuela de Ingenieria y Ciencias, Monterrey, N.L. 64849, Mexico;* orcid.org/0000-0002-9512-7674; Email: adrianap@tec.mx

Authors

Shirley Mora-Godínez − *Tecnologico de Monterrey, Escuela de Ingenieria y Ciencias, Monterrey, N.L. 64849, Mexico*

Flavio F. Contreras-Torres − *Tecnologico de Monterrey, The Institute for Obesity Research, Monterrey, N.L. 64849, Mexico;* orcid.org/0000-0003-2375-131X

Complete contact information is available at: https://pubs.acs.org/10.1021/acsomega.3c01914

Author Contributions

S.M.-G. performed the conceptualization, methodology, formal analysis, investigation, writing of the original draft, and review and editing. F.F.C.-T. contributed to the methodology, resources, and review and editing. A.P. contributed to the methodology, resources, writing of the original draft and review and editing, supervision, project administration, and funding acquisition.

Funding

This study was funded by the CONACYT Mexican National Council for Research and Technology (SEP no. 255612), which also granted a doctoral scholarship to author S.M.-G. (no. 827922) and Tecnologico de Monterrey Research Funding Program (GIEE EICIM 01).

Notes

The authors declare no competing financial interest.

ACKNOWLEDGMENTS

The authors would like to acknowledge Centro de Biotecnología FEMSA, Tecnologico de Monterrey, for their support with laboratory facilities.

REFERENCES

(1) Bruna, T.; Maldonado-Bravo, F.; Jara, P.; Caro, N. Silver nanoparticles and their antibacterial applications. *Int. J. Mol. Sci.* **2021**, *22*, 7202.

(2) Navarro-Gallón, S. M.; Alpaslan, E.; Wang, M.; Larese-Casanova, P.; Londoño, M. E.; Atehortúa, L.; Pavón, J. J.; Webster, T. J. Characterization and study of the antibacterial mechanisms of silver nanoparticles prepared with microalgal exopolysaccharides. *Mater. Sci. Eng., C* **2019**, *99*, 685−695.

(3) Patel, V.; Berthold, D.; Puranik, P.; Gantar, M. Screening of cyanobacteria and microalgae for their ability to synthesize silver nanoparticles with antibacterial activity. *Biotechnol. Rep.* **2015**, *5*, 112−119.

(4) Khanna, P.; Kaur, A.; Goyal, D. Algae-based metallic nanoparticles: Synthesis, characterization and applications. *J. Microbiol. Methods* **2019**, *163*, 105656.

(5) Ahmad, S.; Munir, S.; Zeb, N.; Ullah, A.; Khan, B.; Ali, J.; Bilal, M.; Omer, M.; Alamzeb, M.; Salman, S. M.; Ali, S. Green nanotechnology: a review on green synthesis of silver nanoparticles — an ecofriendly approach. *Int. J. Nanomed.* **2019**, *14*, 5087−5107.

(6) Soleimani, M.; Habibi-Pirkoohi, M. Biosynthesis of silver nanoparticles using Chlorella vulgaris and evaluation of the antibacterial efficacy against Staphylococcus aureus. *Avicenna J. Med. Biotechnol.* **2017**, *9*, 120−125.

(7) Kashyap, M.; Samadhiya, K.; Ghosh, A.; Anand, V.; Shirage, P. M.; Bala, K. Screening of microalgae for biosynthesis and optimization of Ag/AgCl nano hybrids having antibacterial effect. *RSC Adv.* **2019**, *9*, 25583−25591.

(8) Aziz, N.; Fatma, T.; Varma, A.; Prasad, R. Biogenic synthesis of silver nanoparticles using Scenedesmus abundans and evaluation of their antibacterial activity. *J. Nanopart.* **2014**, *2014*, 1−6.

(9) Solovchenko, A.; Gorelova, O.; Selyakh, I.; Pogosyan, S.; Baulina, O.; Semenova, L.; Chivkunova, O.; Voronova, E.; Konyukhov, I.; Scherbakov, P.; Lobakova, E. A novel CO2-tolerant symbiotic Desmodesmus (Chlorophyceae, Desmodesmaceae): Acclimation to and performance at a high carbon dioxide level. *Algal Res.* **2015**, *11*, 399−410.

(10) Premaratne, M.; Liyanaarachchi, V. C.; Nishshanka, G. K. S. H.; Nimarshana, P. H. V.; Ariyadasa, T. U. Nitrogen-limited cultivation of locally isolated Desmodesmus sp. for sequestration of CO2 from simulated cement flue gas and generation of feedstock for biofuel production. *J. Environ. Chem. Eng.* **2021**, *9*, 105765.

(11) Cheng, Y. S.; Labavitch, J. M.; VanderGheynst, J. S. Elevated CO2 concentration impacts cell wall polysaccharide composition of green microalgae of the genus Chlorella. *Lett. Appl. Microbiol.* **2015**, *60*, 1−7.

(12) Mora-Godínez, S.; Abril-Martínez, F.; Pacheco, A. Green synthesis of silver nanoparticles using microalgae acclimated to high CO2. *Mater. Today: Proc.* **2022**, *48*, 5−9.

(13) Lara-Gil, J. A.; Alvarez, M. M.; Pacheco, A. Toxicity of flue gas components from cement plants in microalgae CO 2 mitigation systems. *J. Appl. Phycol.* **2014**, *26*, 357−368.

(14) Ahmed, E. A.; Hafez, A.; Ismail, F.; Elsonbaty, M.; Abbas, H.; Eldin, R. S. Biosynthesis of silver nanoparticles by Spirulina platensis and Nostoc sp. *Glob. Adv. Res. J. Microbiol.* **2015**, *4*, 36−49.

(15) Govindaraju, K.; Basha, S. K.; Kumar, V. G.; Singaravelu, G. Silver, gold and bimetallic nanoparticles production using single-cell protein (Spirulina platensis) Geitler. *J. Mater. Sci.* **2008**, *43*, 5115−5122.

(16) Muthusamy, G.; Thangasamy, S.; Raja, M.; Chinnappan, S.; Kandasamy, S. Biosynthesis of silver nanoparticles from Spirulina microalgae and its antibacterial activity. *Environ. Sci. Pollut. Res.* **2017**, *24*, 19459−19464.

(17) UTEX, 2009. BG-11 Medium, The Culture Collection of Algae, Austin, TX. Available from http://utex.org/products/bg-11-medium (accessed October 2015).

(18) Grace, C. E. E.; Lakshmi, P. K.; Meenakshi, S.; Vaidyanathan, S.; Srisudha, S.; Mary, M. B. Biomolecular transitions and lipid accumulation in green microalgae monitored by FTIR and Raman analysis. *Spectrochim. Acta, Part A* **2020**, *224*, 117382.

(19) Stehfest, K.; Toepel, J.; Wilhelm, C. The application of micro-FTIR spectroscopy to analyze nutrient stress-related changes in biomass composition of phytoplankton algae. *Plant Physiol. Biochem.* **2005**, *43*, 717−726.

(20) Pezzotti, G. Raman spectroscopy in cell biology and microbiology. *J. Raman Spectrosc.* **2021**, *52*, 2348−2443.

(21) Movasaghi, Z.; Rehman, S.; Rehman, I. U. Raman spectroscopy of biological tissues. *Appl. Spectrosc. Rev.* **2007**, *42*, 493−541.

(22) Movasaghi, Z.; Rehman, S.; ur Rehman, D. I. Fourier transform infrared (FTIR) spectroscopy of biological tissues. *Appl. Spectrosc. Rev.* **2008**, *43*, 134−179.

(23) Patil, L.; Kaliwal, B. Effect of CO2 concentration on growth and biochemical composition of newly isolated indigenous microalga Scenedesmus bajacalifornicus BBKLP-07. *Appl. Biochem. Biotechnol.* **2017**, *182*, 335−348.

(24) Ptak, S. H.; Sanchez, L.; Fretté, X.; Kurouski, D. Complementarity of Raman and Infrared spectroscopy for rapid characterization of fucoidan extracts. *Plant Methods* **2021**, *17*, 130.

(25) Wiercigroch, E.; Szafraniec, E.; Czamara, K.; Pacia, M. Z.; Majzner, K.; Kochan, K.; Kaczor, A.; Baranska, M.; Malek, K. Raman and infrared spectroscopy of carbohydrates: A review. *Spectrochim. Acta, Part A* **2017**, *185*, 317−335.

(26) Babiak, W.; Krzemińska, I. Extracellular polymeric substances (EPS) as microalgal bioproducts: A review of factors affecting EPS

synthesis and application in flocculation processes. *Energies* **2021**, *14*, 4007.
(27) Liu, L.; Pohnert, G.; Wei, D. Extracellular metabolites from industrial microalgae and their biotechnological potential. *Mar. Drugs* **2016**, *14*, 191.
(28) Patwal, T.; Baranwal, M. Scenedesmus acutus extracellular polysaccharides produced under increased concentration of sulphur and phosphorus exhibited enhanced proliferation of peripheral blood mononuclear cells. *3 Biotech* **2021**, *11*, 171.
(29) Zhang, J.; Liu, L.; Ren, Y.; Chen, F. Characterization of exopolysaccharides produced by microalgae with antitumor activity on human colon cancer cells. *Int. J. Biol. Macromol.* **2019**, *128*, 761−767.
(30) Bafana, A. Characterization and optimization of production of exopolysaccharide from Chlamydomonas reinhardtii. *Carbohydr. Polym.* **2013**, *95*, 746−752.
(31) Di Pippo, F.; Ellwood, N. T.; Gismondi, A.; Bruno, L.; Rossi, F.; Magni, P.; De Philippis, R. Characterization of exopolysaccharides produced by seven biofilm-forming cyanobacterial strains for biotechnological applications. *J. Appl. Phycol.* **2013**, *25*, 1697−1708.
(32) Castro, L.; Blázquez, M. L.; Muñoz, J. A.; González, F.; Ballester, A. Biological synthesis of metallic nanoparticles using algae. *IET Nanobiotechnol.* **2013**, *7*, 109−116.
(33) Dağlıoğlu, Y.; Yılmaz Öztürk, B. A novel intracellular synthesis of silver nanoparticles using Desmodesmus sp. (Scenedesmaceae): different methods of pigment change. *Rend. Sedute Accad. Naz. Lincei, Cl. Sci. Fis., Mat. Nat.* **2019**, *30*, 611−621.
(34) Jena, J.; Pradhan, N.; Nayak, R. R.; Dash, B. P.; Sukla, L. B.; Panda, P. K.; Mishra, B. K. Microalga Scenedesmus sp.: a potential low-cost green machine for silver nanoparticle synthesis. *J. Microbiol. Biotechnol.* **2014**, *24*, 522−533.
(35) Ebrahiminezhad, A.; Bagheri, M.; Taghizadeh, S. M.; Berenjian, A.; Ghasemi, Y. Biomimetic synthesis of silver nanoparticles using microalgal secretory carbohydrates as a novel anticancer and antimicrobial. *Adv. Nat. Sci.: Nanosci. Nanotechnol.* **2016**, *7*, 015018−015019.
(36) Hamida, R. S.; Ali, M. A.; Alkhateeb, M. A.; Alfassam, H. E.; Momenah, M. A.; Bin-Meferij, M. M. Algal-Derived Synthesis of Silver Nanoparticles Using the Unicellular *ulvophyte* sp. MBIC10591: Optimisation, Characterisation, and Biological Activities. *Molecules* **2022**, *28*, 279.
(37) Hamida, R. S.; Ali, M. A.; Almohawes, Z. N.; Alahdal, H.; Momenah, M. A.; Bin-Meferij, M. M. Green Synthesis of Hexagonal Silver Nanoparticles Using a Novel Microalgae Coelastrella aeroterrestrica Strain BA_Chlo4 and Resulting Anticancer, Antibacterial, and Antioxidant Activities. *Pharmaceutics* **2022**, *14*, 2002.

https://doi.org/10.1021/acsomega.3c01914
ACS Omega 2023, 8, 21969−21982